# On the Mechanism for Nitrate Formation via the Peroxy Radical + NO Reaction

**Jieyuan Zhang,[†] Tim Dransfield,[‡] and Neil M. Donahue*[,§]**

*Departments of Chemistry and Chemical Engineering, Carnegie Mellon University, Pittsburgh, Pennsylvania 15213, and Harvard University, Cambridge, Massachusetts 02138*

*Received: May 3, 2004; In Final Form: August 4, 2004*

We present a master equation study of organic nitrate formation from the peroxy radical ($RO_2$) + NO reaction. The mechanism is constrained by both quantum chemical calculations of the potential energy surface and existing yield data. This mechanism displays heretofore unrecognized features of the system, including distinct conformers of a critical peroxynitrite (ROONO) intermediate that do not interconvert and a dual falloff behavior driven by collisional stabilization in multiple wells. These features have significant implications for atmospheric chemistry; in particular, only a fraction of the ROONO intermediates may easily isomerize to nitrates, resulting in a limit to total nitrate production. Existing mechanisms, extrapolated to low temperature and high pressure, produce nitrate almost exclusively. As a consequence, hydrocarbon oxidation sequences based on these mechanisms do not propagate radical chemistry, which is inconsistent with available experimental data. To reproduce observed nitrate yields, we model a transition state from the ROONO intermediate to $RONO_2$ that differs considerably from the few found in computational studies. Specifically, the data require that this transition state energy lie well below the energy of separated radical products (RO + $NO_2$), while computational studies find the transition state at higher energies. A second feature of yield data is difficult to model; to enable collisional stabilization of $C_5$ systems, as observed, we reduce the unimolecular decomposition rate constants from the ROONO intermediate by a factor that is at the far end of the plausible range. However, with these experimental constraints in place, the model successfully reproduces multiple features of existing data quantitatively, including both high- and low-pressure asymptotes to nitrate production as well as the observed shifting of pressure falloff curves with carbon number. Consequently, we present a new parametrization of nitrate yields, providing interpolation equivalent to existing parametrizations but dramatically improved extrapolation behavior.

## 1. Introduction

*If one heretofore unobserved reaction intermediate cannot explain published data, why not invoke two?*

The reaction of peroxy radicals ($RO_2$) with nitric oxide (NO) sits in the very center of atmospheric chemistry. On one hand, it may yield radical products, alkoxy radicals (RO) and $NO_2$, effectively producing ozone after $NO_2$ photolysis. On the other hand, it may yield nitrates ($RONO_2$), effectively terminating the radical chain reaction in the atmosphere. It is widely accepted that both channels share a common intermediate, a peroxy nitrite (ROONO), whose subsequent decomposition governs the branching between radicals and nitrate, as shown in the following sequence:[1,2]

$$RO_2 + NO \rightarrow ROONO \quad (1)$$

$$ROONO \rightarrow RO + NO_2 \quad (2)$$

$$\rightarrow RONO_2 \quad (3)$$

What has not been recognized is that two generally distinct conformers of the ROONO intermediate have quite separate chemical behaviors and fates. We will refer to these conformers as *cis*- and *trans*-ROONO (describing the O−O−N−O conformation). In particular, the isomerization between these two forms is quite slow, compared to the other reactions open to each conformer, and only one conformer can easily isomerize to become a nitrate. Thus one conformer connects only to the radical products, while the other connects to both radicals and nitrates. We shall argue that this easily isomerized ROONO is the trans form, though the only important conclusion is that the conformers behave differently. The first purpose of this paper is to establish this assertion and to discuss its implications.

The second purpose of this paper is to build the case that the observed pressure dependence for nitrate yields (for all but the very smallest species) is due to the collisional stabilization of these ROONO intermediates and their subsequent, rapid, thermal decomposition. Nitrate yields are thus controlled by three factors: (1) the initial branching of the $RO_2$ + NO reaction between *cis*- and *trans*-ROONO; (2) the ratio of nitrate to radical formation for *trans*-ROONO at high (reactant) energy (which controls the low-pressure production of nitrate); and (3) the critical energy difference between the nitrate and radical pathways out of *trans*-ROONO (which controls the high-pressure limit and the temperature dependence of nitrate formation). An intriguing consequence of this is that the puzzling variation of nitrate yields among different classes of peroxy radicals (primary, secondary, and tertiary alkyl-peroxy[3]; $\beta$-hydroxy-peroxy radicals[4−7]) may be governed in large measure by the initial branching between *cis*- and *trans*-ROONO.

* To whom correspondence should be addressed. E-mail: nmd@andrew.cmu.edu.
[†] Carnegie Mellon University, Department of Chemical Engineering.
[‡] Harvard University, Department of Chemistry and Chemical Biology.
[§] Carnegie Mellon University, Department of Chemistry.

10.1021/jp048096x CCC: $27.50 
Published on Web 09/25/2004

The emphasis of this work is *not* computation of the potential energy surface (PES). In fact, we will assert that two key aspects of the reaction, the conformers of ROONO and the transition state between ROONO and $RONO_2$, are sufficiently challenging that even state-of-the-art computational efforts serve only as a rough guide. This is especially true of the ROONO to $RONO_2$ transition state, which appears to be a long-range complex between RO and $NO_2$, where computational methods are pushed beyond their limits. Consequently, our focus will be to make "reasonable" assumptions about these key properties, guided by relatively low-level quantum chemistry, and then to test those assumptions against available data using statistical reaction dynamics (master equation) calculations. Like all of the efforts before this, we shall confront some inconsistencies, but overall we shall present a model for the reaction mechanism that is broadly consistent with available data and computational results.

## 2. Potential Energy Surfaces

Though the basic form of reaction 1 is supported by a broad array of experimental and theoretical evidence, the details have proven inscrutable. In particular, the ROONO intermediate itself has not been observed in the gas phase for R ≠ H, and computational studies have yielded an array of ROONO conformers.[8−15] Furthermore, a convincing transition state from ROONO to $RONO_2$ has not been found; all computed transition states have energies higher than the RO + $NO_2$ decomposition products,[11,13] and, as we shall show, this is inconsistent with experimental observations. The succession of highly electronegative atoms in ROONO makes all computations difficult, and the (presumably) extended nature of the ROONO → $RONO_2$ transition state adds a final degree of difficulty. From the available evidence, we draw two conclusions: (1) the significant conformational isomerization in ROONO is a change from cis to trans in the O−O−N−O; and (2) the transition state energies from each of these two conformers to $RONO_2$ are almost certainly quite different from one another.

Put simply, a transition state from *trans*-ROONO to $RONO_2$ must involve a largely in-plane counter rotation of the $NO_2$ and RO moieties, while a transition state from *cis*-ROONO to $RONO_2$ must involve a largely out-of-plane counter rotation of the same moieties. It is clear that the transition state from *trans*-ROONO to $RONO_2$ is significantly different geometrically from the transition state from *cis*-ROONO to $RONO_2$. It is thus likely that the energies of these two transition states will differ. Here we explore the limit at which only one transition has a low enough energy to compete with other reaction pathways. This is consistent with recent computational work, including high-level calculations for R═H and R═$CH_3$[16] and for the analogous FONO surface.[17] For the calculations reported here, we assumed that any transition states from *cis*-ROONO to $RONO_2$ were effectively closed, with microcanonical rates at all energies much lower than for competing processes such as dissociation to radicals (RO + $NO_2$). The computational work of Houk and co-workers shows that the cis rather than the trans conformer couples more efficiently to $RONO_2$,[16] but this will not alter the results presented here. The important aspect is that only *one* of the conformations leads to nitrate.

For this work, we shall assume that the potential energy surface for reaction R1 is substantially similar for all R, especially when the R falls within a given class (i.e., secondary alkyl radicals). In particular, we shall assume that for the series R = {H, $CH_3$, $C_2H_5$, ..., $C_nH_{2n+1}$}, the only significant changes are in the RO radical energy, with HO (hydroxyl) being unusually high (and thus HOONO being unusually stable), $CH_3O$ being unusually low, and all larger RO being intermediate. This is consistent with accepted heats of formation for peroxy and alkoxy radicals,[10−12,18] the general stability of the $RO_2$ + NO rate constant for various R,[19,20] and the recent work from Lohr and Barker.[13,14] Because the focus here is on nitrate yields for relatively large peroxy radicals (>$C_2$), we shall adopt the suggestion of Barker[14] and use a single potential for all calculations. For the generic potential, we will use the G3 surface from Lohr et al., as it appears to capture the RO energies more accurately.[13] Additionally, we assume a 4000 $cm^{-1}$ isomerization barrier (TS1) from *trans*- to *cis*-ROONO.

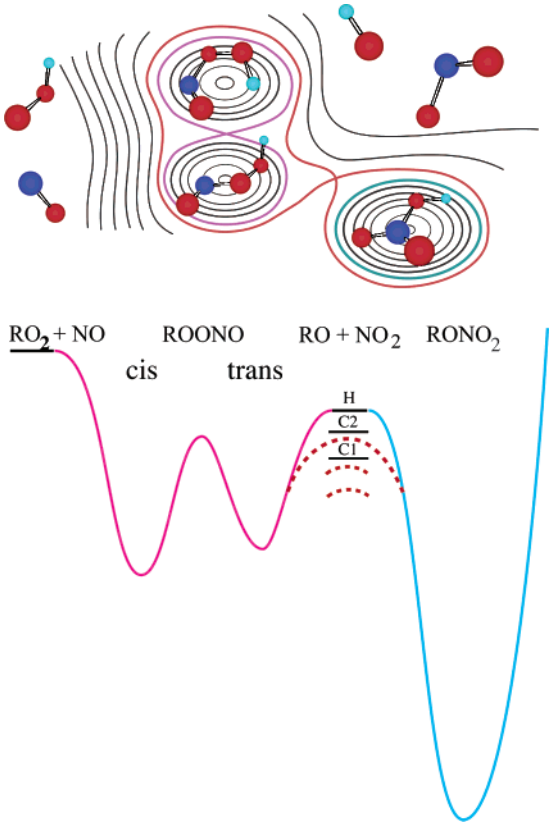


**Figure 1.** Cartoon depiction of the potential energy surface and key species involved in organic nitrate formation. The top panel is a topographical presentation, with ball-and-stick depictions of $RNO_3$ species. O is red, N blue, and R the light-blue half-sized ball. The lower panel shows an approximately scaled energy coordinate for the same surface. Note in particular the considerable difference between the cis and trans conformers of the ROONO intermediate. The cis conformer is cyclic, with hydrogen bond stabilization increasing its stability, while the trans conformer is roughly linear. The cis conformer is obviously geometrically distant from the nitrate ($RONO_2$) isomer, shown to the lower right, while the trans conformer can isomerize to the nitrate with a relatively facile internal rotation of the $NO_2$ group (which nonetheless requires breakage of an O−O bond and formation of an O−N bond). As shown in the lower panel, the energies of the RO + $NO_2$ fragments vary systematically, with H highest, $CH_3$ lowest, and C2 and larger R in between. We assume that the *trans*-ROONO → $RONO_2$ transition state energy (shown as a red dashed line) varies in concert with this. Energies used in this study are shown in Table 1 and Figure 6.

Note that these assumptions are clearly inconsistent with the established evidence that nitrate yields depend on the broad class of peroxy radicals. Something must be driving the different yields, and that must be reflected in the potential energy surface, though the cause may be subtle differences in the cis−trans branching of the initial $RO_2$ + NO reaction. For the purposes of this study, we shall consider secondary peroxy radicals only and add in H and $CH_3$ as "effective" secondary alkyl radicals in order to explore the influence of size to its limits.

**TABLE 1: Comparison of Computational Potential Energies for a Series of R[a]**

| R | $RO_2 + NO$ | *cis*-ROONO[b] | TS1[c] | *trans*-ROONO | $RO + NO_2$ | TS2[d] | $RONO_2$ | reference |
|---|---|---|---|---|---|---|---|---|
| H | 7867 | 0 | 4680 | 745 | 5199 | | −10097 | this work |
| | | 0 | 4440 | 770 | 4060 | 4160 | −10910 | Zhao (ref 16) |
| | | [0] | [4510] | [1120] | [6850] | [7380] | [−10420] | Zhao (ref 16) |
| | | 0 | 4700 | 680 | 3790 | | −10790 | Golden (ref 15) |
| | | (0) | (4970) | (1130) | (6090) | | (−10160) | Golden (ref 15) |
| | 7020 | 0 | | | 3790 | 13620 | −10790 | Lohr (ref 13) |
| | (9090) | (0) | | | (6080) | | (−10160) | Lohr (ref 13) |
| | 9090 | 0 | 5600 | 1050 | 6640 | | −10140 | Donahue (ref 21) |
| $CH_3$ | 6580 | 0 | 4214 | 241 | 1321 | | −10231 | this work |
| | | 0 | 4550 | 460 | 1640 | | −10210 | Zhao (ref 16) |
| | | [0] | [4130] | [490] | [4480] | | [−10460] | Zhao (ref 16) |
| | 6200 | 0 | | | 710 | 11630 | −10460 | Lohr (ref 13) |
| | (8250) | (0) | | | (4220) | | (−10270) | Lohr (ref 13) |
| $C_2H_5$ | 6938 | 0 | 4644 | 535 | 2294 | | −9483 | this work |
| | 6180 | 0 | | | 1340 | 11920 | −10370 | Lohr (ref 13) |
| | (8370) | (0) | | | (4680) | | (−10170) | Lohr (ref 13) |
| *n*-$C_3H_7$ | 6623 | 0 | 4378 | 315 | 1817 | | −9875 | this work |
| | 6160 | 0 | | | 1180 | 11580 | −10420 | Lohr (ref 13) |
| | (8480) | (0) | | | (4520) | | (−10140) | Lohr (ref 13) |
| *i*-$C_3H_7$ | 6492 | 0 | 4573 | 442 | 1665 | | −10074 | this work |
| | 6260 | 0 | | | 1230 | 11770 | −10160 | Lohr (ref 13) |
| | (8540) | (0) | | | (5180) | | (−9980) | Lohr (ref 13) |
| 2-$C_5H_{11}$ | 6637 | 0 | 4957 | 668 | 1732 | | −9703 | this work |
| | 6200 | 0 | | | 1210 | 11280 | −10290 | Lohr (ref 13) |
| R[e] | 6600 | 0 | 4500 | 500 | 5400 | 3870 | −10000 | this work |

[a] Energies (shown in $cm^{-1}$) were calculated using B3LYP/6-31+G(d,p) (this work), B3LYP/6-311++G** (by Zhao et al.,[16] Golden et al.,[15] and Lohr et al.[13]), B3LYP/6-31G** (by Donahue et al.[21]), CBS-QB3 (in square parenthesis by Zhao et al.[16]), or G3 (in parentheses by Golden et al.[15] and Lohr et al.[13]). [b] All the energies are relative to the energy of the *ciscis*-ROONO intermediate. [c] Transition state from *trans*-ROONO to *cis*-ROONO. [d] Transition state from ROONO to $RONO_2$. [e] Energies used in our master equation calculation.

In Figure 1, we show the generic potential energy landscape in a cartoon form, with ball-and-stick representations of the key species. The lower panel of Figure 1 reproduces Figure 1 in our earlier work on OH + $NO_2$,[21,22] with additional product energies depicted for $CH_3O$ and $C_2H_5O$. We also assume that the *trans*-ROONO to $RONO_2$ transition state energy (shown as a red dashed line in Figure 1) varies in conjunction with the RO energies, so that the energy difference between these two states does not change as the RO energy varies. This is because of the presumptive geometry and physics of this unusual transition state, which we shall discuss below.

A critical feature on this potential energy surface is the transition state energy for isomerization between the *cis*- and *trans*-ROONO conformers (TS1 in Table 1). We have computed energies and frequencies for this transition state, along with all of the stable species energies, for the series R = H, $CH_3$, $C_2H_5$, *n*-$C_3H_7$, *i*-$C_3H_7$, and 2-$C_5H_{11}$. Calculations at the B3LYP/6-31+G(d,p) level of theory are summarized in Table 1, along with literature results. Our results are substantially consistent with earlier results.[10−16] Geometries and frequencies are contained in the Supporting Information. The energy difference between the results by Lohr et al. and ours is caused by the smaller basis set used in our computations. Consistent with our earlier work[21] and Golden's work[15] for R = H, the cis−trans isomerization transition state lies approximately 500 $cm^{-1}$ below the energy of separated RO and $NO_2$ at the B3LYP/6-31+G(d,p) level of theory. This is because the extensively delocalized $\pi$-bonding network stabilizing the O−N−O−O moiety is disrupted by the internal rotation. As shown in Table 1, the energy for TS1 remains constant with different basis sets and up to the G3 level of theory for the HOONO system; we therefore conclude that our energies for this transition state are sufficiently accurate for the following calculations. Our assumed TS1 energy (4000 $cm^{-1}$ relative to *trans*-ROONO) is also consistent with a recently published high-level computation.[16]

Even more important to the issue at hand is the isomerization transition state from *trans*-ROONO to $RONO_2$. We will draw on data, specifically the temperature dependence of high-pressure limits, to constrain the difference in transition state energies between the isomerization and dissociation to radicals ($RO + NO_2$). This will show that the isomerization transition state lies approximately 2200 K (1530 $cm^{-1}$) lower than the radical products, which differs significantly from computational results. The computed transition state energy has, however, been steadily declining in recent years.[11,13,16] This transition state almost certainly involves the partial dissociation of the RO−ONO, followed by $NO_2$ rotation to complete the isomerization. These assertions about the geometry and energy are both broadly consistent with the conclusions of Barker et al.[14] Given the large error in energy and the extended geometry, there is little reason to believe that the computational results significantly constrain either the energy or geometry of this transition state. Instead, because the data show a consistent energy difference between the transition state and the radical products' energies, we shall assume that these two energies are highly correlated, as shown in Figure 1, with the transition state lying at a fixed 2200 K below the radical products. As discussed earlier, we will assume that only the *trans*-ROONO conformer has a low-energy transition state to $RONO_2$ and then examine the consequences of this assumption.

### 3. Literature Data

This analysis relies completely on published nitrate yield data from various precursors. Our focus is on the pressure and temperature dependence of the yields, as this provides the most mechanistic information. The primary data set thus comes from Aschmann and Atkinson.[1,23] There are abundant data on nitrate yields from various peroxy radicals (most of them secondary) at pressures ranging from 0.08 to 1 atm and temperatures ranging from 282 to 323 K. They found that nitrate yields are generally consistent for a given class of peroxy radicals (i.e., secondary alkylperoxy radicals), though yields increase systematically with increasing carbon number. Aschmann and Atkinson report nitrate yields as a function of number density. Assuming that

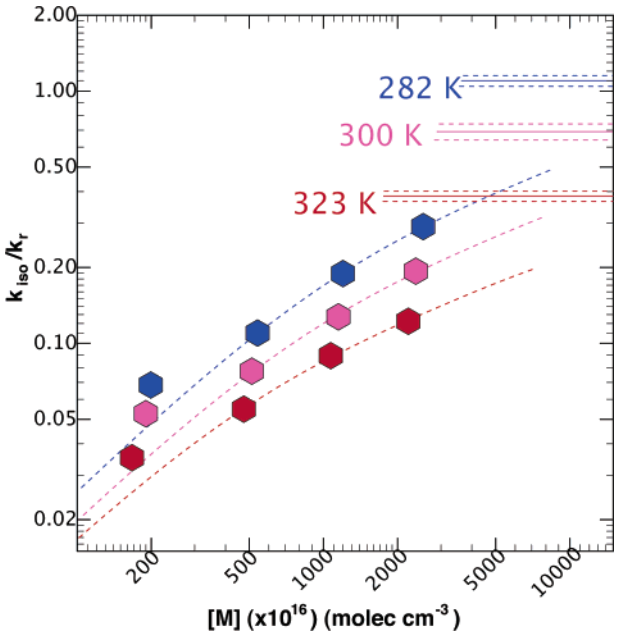


**Figure 2.** Branching versus pressure (number density) at three temperatures for 3-methyl-2-pentylperoxy + NO, from Atkinson et al. (ref 1). Data are shown as the branching as a ratio of isomerization (nitrate formation) over radical production (RO + $NO_2$). Dashed lines show pressure dependent fits to data from each temperature, excluding the lowest pressure point in each case, and short horizontal lines show the corresponding high-pressure limits, beginning at $M_c$ in each case.

two pathways (R2 and R3) proceed with rates $k_{iso}$ (isomerization) and $k_r$ (radical formation), this is equivalent to

$$y_n = \frac{k_{iso}}{k_{iso} + k_r}$$

However, we shall consider instead the branching ratio

$$r_n = \frac{k_{iso}}{k_r}$$

because it is more directly related to the loss processes of a presumed ROONO intermediate.

Our first objective is to constrain the ROONO to $RONO_2$ transition state energy. Presuming that the pressure dependence is driven by ROONO stabilization, this energy is most easily found from the high-pressure limits of nitrate production. Pressure-dependent data are easily fit to the standard reduced falloff form of Troe[24] (we here use the common "JPL" simplification[25] of $F_c = 0.6$). Figure 2 shows a representative result, in this case for 3-methyl-2-pentyl nitrate. Each temperature is fit independently, and in each case a high-pressure limiting value is found at a pressure substantially higher than the extent of the data. These high-pressure limits are thus relatively uncertain, individually.

One common problem affects data for most compounds; very often the lowest pressure data point deviates significantly from the best-fit curve. In fact, these points (typically at 50 Torr, [M] $\approx 2 \times 10^{18}$ molecules $cm^{-3}$) need to be excluded from most falloff fits to get sensible results. They are more consistent with a low-pressure asymptote to nitrate yields with a value of order 0.04 than with a continuous, linear falloff toward zero yield. The low-pressure asymptote will be a major feature of our subsequent theoretical discussion. Once these data are excluded, the yield data are generally fit with good precision, consistently displaying the behavior shown in Figure 2.

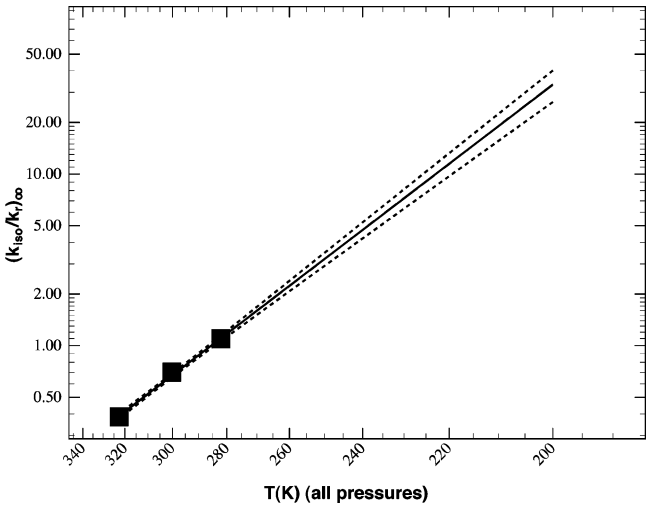


**Figure 3.** Arrhenius fits of the high-pressure limits to the yield ratio $k_{iso,\infty}/k_{r,\infty}$ shown in Figure 2. The result is plotted down to 200 K, to emphasize the very high ratio (corresponding to negligible radical yields) suggested at low temperatures.

These results are not significantly different from the analysis performed by Aschmann and Atkinson.[1,23] At this point, however, we will make our first significant assumption, to be tested for consistency by the available data and ultimately by master equation calculations as well: *We assume that the pressure dependence reflects collisional stabilization of the peroxynitrite intermediate shown in reactions 2 and 3. Furthermore, we assume that the temperature dependence of the high-pressure limits obtained in these falloff fits reflects the thermal decomposition of this intermediate.* Specifically, at the high-pressure limit, the radical and isomerization pathways will each have Arrhenius unimolecular rate constants from the ROONO intermediate:

$$k_{iso} = A_i\, e^{-Ea_i/(RT)} \quad (4)$$

$$k_r = A_r\, e^{-Ea_r/(RT)} \quad (5)$$

so

$$\frac{k_{iso}}{k_r} = \frac{A_i}{A_r} e^{-\Delta Ea/(RT)} = A_{i,r}\, e^{-\Delta Ea/(RT)} \quad (6)$$

Consequently, we fit the high-pressure limits for each reaction to an Arrhenius form, as shown in Figure 3 for 3-methyl-2-pentyl nitrate. The quality of these fits varies; the one shown in Figure 3 is one of the more precise. However, the fits uniformly show a strong negative temperature dependence, indicating that the isomerization barrier lies well *below* the radical dissociation barrier.

Because the individual fits lack precision, it is the aggregate behavior of the Arrhenius fits that provides a constraint. Consequently, there are sufficient data only for secondary peroxy radicals. When we plot the barrier differences versus *A*-factor ratios on a semilog plot (in *x*) for each secondary peroxy radical reaction (Figure 4), while there is a distribution of values, they fall along a line of constant yield at 300 K (shown on the plot). This is again consistent with the conclusions of Aschmann and Atkinson, that each class of peroxy radical results in a common nitrate yield behavior. However, we can draw a more precise conclusion from this behavior. The errors in Ea and ln *A* are highly correlated, and so standard error bars do not suit the presentation; rather we show the highly flattened error ellipses

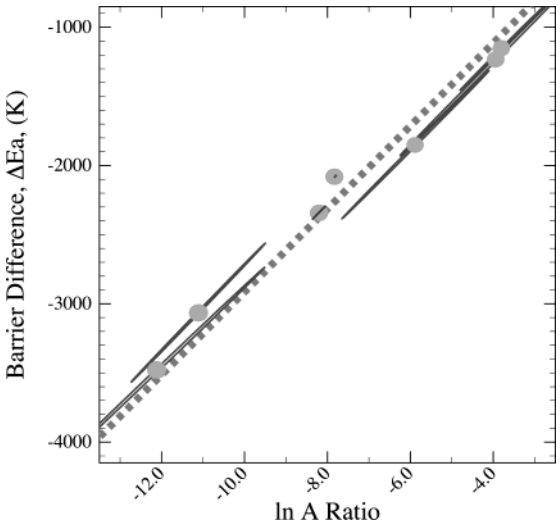


**Figure 4.** Arrhenius results (ΔEa vs $A_{i,r}$) for all secondary peroxy radical organic nitrate formation reactions (2-pentylperoxy, 3-pentylperoxy, 2-methyl-3- butylperoxy, 3-methyl-2-pentylperoxy, 2-heptylperoxy, 3-heptylperoxy, 4- heptylperoxy). The dashed line is a constant yield contour at 300 K. Error ellipses show high correlation between these two fit parameters, corresponding to a constant 300 K nitrate yield at the high-pressure limit. A precision-weighted average gives ΔEa ≃ −2200 K (−1530 cm$^{-1}$) and $A_{i,r} \simeq 5 \times 10^{-4}$.

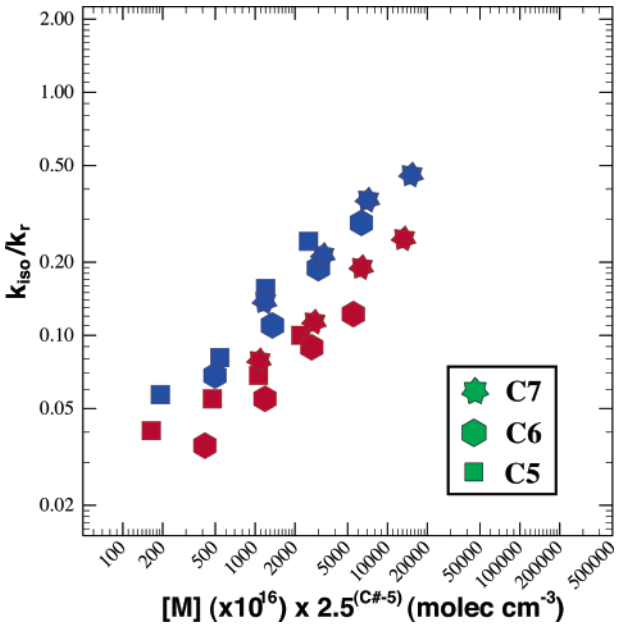


**Figure 5.** Pressure-dependent nitrate yields for $C_5$ (2-methyl-3-butyl), $C_6$ (3-methyl-2- pentyl), and $C_7$ (4-heptyl) nitrates, shifted to reflect the effect of increasing carbon number. Yields are shifted by the simple formula $P = P_0 \times 2.5^{(n-5)}$, where $n$ is carbon number.

for each value. These are so flattened by the nearly unit correlation of errors that they essentially form diagonal error bars, aligned parallel to the 300 K isoyield line. The two most precise results are for 3-methyl-2-pentyl peroxy and 2-pentyl peroxy + NO, and each lies near the center of the figure. It is hard to believe that serendipity would place these values on an isoyield line; far more likely is that all of the reactions have a common $A$ and ΔEa. The most probable result, based on the precision of the fits, is $A_{i,r} = 5 \times 10^{-4}$, ΔEa = −2200 K (−1530 cm$^{-1}$). Our interpretation of the increasing yields observed at low temperature is thus that the barrier for ROONO isomerization to nitrates lies consistently some 2200 K below the dissociation threshold of ROONO to RO and $NO_2$.

A final constraint applies to the overall size dependence of nitrate formation. As noted by Atkinson,[26,27] nitrate yields increase with size systematically. This is shown in Figure 5, in which the pressures for secondary peroxy radicals with carbon numbers different from 5 are shifted by a simple formula, $P = P_0 \times 2.5^{(n-5)}$, where $n$ is carbon number. This shows that the yields are reasonably consistent with increasing carbon number and that the main effect of additional carbons is to increase collisional stabilization, as we would expect from RRKM theory. Increasing the carbon number by 5 effectively increases the lifetime by a factor of about 100, hence moving the p(1/2) point to pressures that are lower by a factor of about 100.

This aggregate assessment of experimental data at the high-pressure limit and computational potential energy surfaces thus provides the broad constraints for our analysis. We have made no effort to infer a branching in the initial reaction forming *cis*- and *trans*-ROONO, as there are essentially no data to constrain this and a computational result is equally difficult to achieve. However, as we shall see, the general constraints provided so far are sufficient.

## 4. Theoretical Section

**4.1. Microcanonical Rate Constants.** The core of this work lies in estimating the microcanonical rate constants for the various transition states shown in Figure 1. Structures and frequencies for all stable species are based on density functional calculations (B3LYP/6-31+G(d,p)) for the series R = H, $CH_3$, $C_2H_5$, *n*-$C_3H_7$, *i*-$C_3H_7$, and 2-$C_5H_{11}$, as presented in the Table 1 and the Supporting Information. For each R, there are five important, stable geometries: three wells ($RONO_2$, *trans*-ROONO, and *cis*-ROONO) and two sets of separated radicals ($RO_2$ + NO and RO + $NO_2$), ignoring minor conformers. The interesting feature is that there are two groups of ROONO intermediates (cis and trans) for each R. All the *cis*-ROONO intermediates have nearly the same energy, and all the *trans*-ROONO intermediates have nearly the same energy. There are seven transition states to connect all the five stable geometries: five connect separated radicals to the three wells (each ROONO conformer connects to both $RO_2$ + NO and RO + $NO_2$, and $RONO_2$ connects to RO + $NO_2$), and two more connect wells in a serial chain from *cis*-ROONO to *trans*-ROONO to $RONO_2$). All the results are broadly consistent with Lohr and Barker.[13,14] Because our main purpose is to explore the effects of increasing size on these systems, we do *not* rely on computational energies and frequencies for larger carbon number systems. Rather, we have extensively mapped the $CH_3ONO_2$ potential energy surface, as discussed earlier, and extended these results by simply adding successive methylene groups in a systematic way to the model system. Each additional $CH_2$ adds 9 degrees of freedom to every structure in the system, which we model as 2 C−H stretches ($\nu$ = 3090 and 3120 cm$^{-1}$), 3 C−H bends ($\nu$ = 1310, 1410, and 1540 cm$^{-1}$), 1 C−C stretch ($\nu$ = 910 cm$^{-1}$), 2 C−C bends ($\nu$ = 820 and 420 cm$^{-1}$, the second reflecting slow "backbone" bending), and 1 conformational torsion (a hindered rotor with $\nu$ = 80 cm$^{-1}$ and a 3 kcal/mol barrier).

The critical structures on the PES are the transition states for radical formation (RO + $NO_2$) out of each of the three major wells (*cis*- and *trans*-ROONO and $RONO_2$) and the isomerization transition states (*cis*- to *trans*-ROONO and *trans*-ROONO to $RONO_2$). Following Barker et al.,[14] we approximate the radical formation pathways using a hindered Gorin model. The model locates the transition state at the centrifugal barrier, as calculated by the equation[28]

$$r^+ = r_{eq}\left(\frac{6D_e}{RT}\right)^{1/6} \quad (7)$$

The location of the transition state is thus weakly temperature dependent. We specify five transition state modes as hindered internal rotors; for ROONO decomposition, three modes correspond to RO fragment hindered rotations and two modes correspond to $NO_2$ rotation. The "unhindered" moments, $I_0$, of these modes are calculated using the method of Herschbach,[29] based on distances from an axis intersecting the fragment center of mass but parallel to the breaking bond. These moments are reported in the Supporting Information. The hindered moments of inertia, $I^+$, are calculated at a stretched bond distance $r^+$ based on a formula suggested by Abbatt:[28]

$$I^+ = I_0(1 - e^{-\gamma(r^+ - r_{eq})}) \quad (8)$$

where $\gamma$ is a free parameter, representing the degree of hindrance. $I^+$ increases as $\gamma$ increases, with $I^+ = I_0$ when $\gamma \rightarrow \infty$. For our base-case simulations, we use $\gamma = 0.08$ for all loose transition states, corresponding to $(1 - \eta)^{1/2} \approx 0.14$ in the restricted Gorin model by Smith and Golden,[30] which is similar to the value used by Barker.[14]

Because the energy we infer for the nitrate formation transition state differs so markedly from computational results,[11] we have instead developed a crude model of this transition state structure based on extension of the O−O bond in ROONO, in conjunction with an in-plane counter rotation leading toward $RONO_2$. The structure of the transition state is similar to the structure of the dissociation transition state, but with the N atom twisted toward the O atom of the RO group. We assume that this transition state is sufficiently tight to treat the internal modes as vibrations, with frequencies estimated based on the $CH_3ONO_2$ frequencies. We keep 12 frequencies corresponding to $CH_3O$ and $NO_2$ in $CH_3ONO_2$ unchanged and then loosen the 5 frequencies left in $CH_3ONO_2$ (excluding the reaction coordinate) by multiplying each by a factor $\zeta = 0.4$.[31] The 5 frequencies include 2 C−O−N−O torsions ($\nu = 130$ cm$^{-1}$ and $\nu = 370$ cm$^{-1}$), 1 O−N−O bend ($\nu = 570$ cm$^{-1}$), 1 N−O stretch ($\nu = 640$ cm$^{-1}$), and 1 asymmetric C−O−N stretch ($\nu = 1020$ cm$^{-1}$). The factor $\zeta$ is effectively a free parameter related to $A_\infty$, which allows us to adjust this model given the constraints imposed by the nitrate yield data.

The transition state from *trans*- to *cis*-ROONO is relatively tight, so we use our computational results. Consistent with the general PES we are employing, we assume that this transition state energy is uniformly 4000 cm$^{-1}$ above the *trans*-ROONO energy, or approximately 900 cm$^{-1}$ below the dissociation threshold to radical products (RO + $NO_2$).

Each of these transition state structures features significant extension of at least one critical bond, and so we must consider conservation of angular momentum. Consistent with the relatively crude nature of these model transition states, we use a correction based on two adiabatic external rotations.[14] Ultimately, the microcanonical rate constants are

$$k(E) = c\frac{G(E - E_0)}{\rho(E)} \quad (9)$$

with $E$ in cm$^{-1}$. To calculate sums and densities of states, we use the densum program developed by John Barker.[32]

In Figure 6, we present our microcanonical results for reactions leading from the *trans*-ROONO well in the $C_5$ system used as a base case throughout this paper. Note that the figure shows rate constants on the $x$ axis to maintain consistency with our PES figures. The important portion of the PES is shown in Figure 6, as is a typical initial energy distribution for the flux into the *trans*-ROONO well. The important features are as follows:

1. The back reaction to $RO_2$ + NO is of minimal significance, reaching a maximum of a few percent of the total rate constant at very high energies.

2. The isomerization to *cis*-ROONO is even less important, *never* exceeding 1% of the total rate constant at any energy.

3. The competition between isomerization to $RONO_2$ and dissociation to radicals is more complex. At low energy (below the dissociation limit) isomerization dominates, but once the energy exceeds the radical dissociation limit, the dissociation rate constant rapidly exceeds the isomerization rate constant; at typical initial energies for the $RO_2$ + NO reaction, radical formation is roughly an order of magnitude faster than isomerization to $RONO_2$.

The infinite energy $A$-factors for reactions 2 and 3 are $2 \times 10^{16}$ and $1.5 \times 10^{14}$ s$^{-1}$, respectively. Each of these is approximately 1 order of magnitude less than the values calculated by Barker and Lohr.[14] The lower $A$-factor for both reactions reflects the high uncertainty and numerous assumptions associated with loose transition states such as those under consideration here. In addition, we have assumed a somewhat tighter nitrate isomerization transition state, which drives the crossover point of these critical reactions to lower energy. Under these conditions, the system strongly favors radicals at the high energies associated with the initial reactants but strongly favors nitrate formation at thermal energies (in the ROONO well). The qualitative implications of these microcanonical rate constants are clear: First, our assumption that the cis and trans isomers of ROONO are disconnected is consistent with our calculated rate constants. Second, at low pressures, where collisional stabilization is negligible, radical product formation should dominate over nitrate formation. Finally, at high pressure, once the *trans*-ROONO intermediate is collisionally stabilized, the subsequent thermal decomposition will favor nitrate formation because of the significantly lower barrier for this pathway.

**4.2. Master Equation Calculations.** To quantitatively calculate nitrate yields, we employ a time-dependent master equation solution based on matrix inversion.[33,34] The time-dependent population $\mathbf{N} = N(e)$ of an intermediate is

$$\frac{d\mathbf{N}}{dt} = R\mathbf{F} - [\omega(\mathbf{I} - \mathbf{P}) + \sum_i \mathbf{K}_i]\mathbf{N} \equiv R\mathbf{F} - \mathbf{J}\mathbf{N} \quad (10)$$

in which $R$ is the overall time-independent rate of intermediate formation, $\mathbf{F}$ is the vibrational population distribution of the nascent intermediate, $\mathbf{P}$ is the (normalized) energy transfer matrix, $\mathbf{I}$ is the unit matrix, $\omega$ is the collision frequency, and $\mathbf{K}_i$ is a diagonal matrix of unimolecular rate constants for the $i$th channel. The steady-state solution of eq 10 yields the simple expression $\mathbf{N} = \mathbf{J}^{-1}R\mathbf{F}$. The time-dependent solution is given in terms of the eigenvectors ($\mathbf{U}$) and eigenvalues ($\Lambda$) of $\mathbf{J}$:

$$\frac{\mathbf{N}}{R} = \mathbf{U}\mathbf{L}\mathbf{U}^{-1}\mathbf{F} \quad (11)$$

where $\mathbf{L}$ is a diagonal matrix with diagonal elements $i$ equal to $(1 - e^{-\Lambda(i)t})/\Lambda(i)$. Note that $\mathbf{L}(t \rightarrow \infty) \rightarrow \Lambda^{-1}$. The eigenvector associated with the smallest eigenvalue, $\lambda(1)$, corresponds to thermal equilibrium, and thus inclusion of this eigenvector amounts to consideration of thermal decomposition. We can thus include or exclude thermal decomposition by setting $L(1)$ to either $1/\lambda(1)$ or 0. Consequently, we consider two steady-

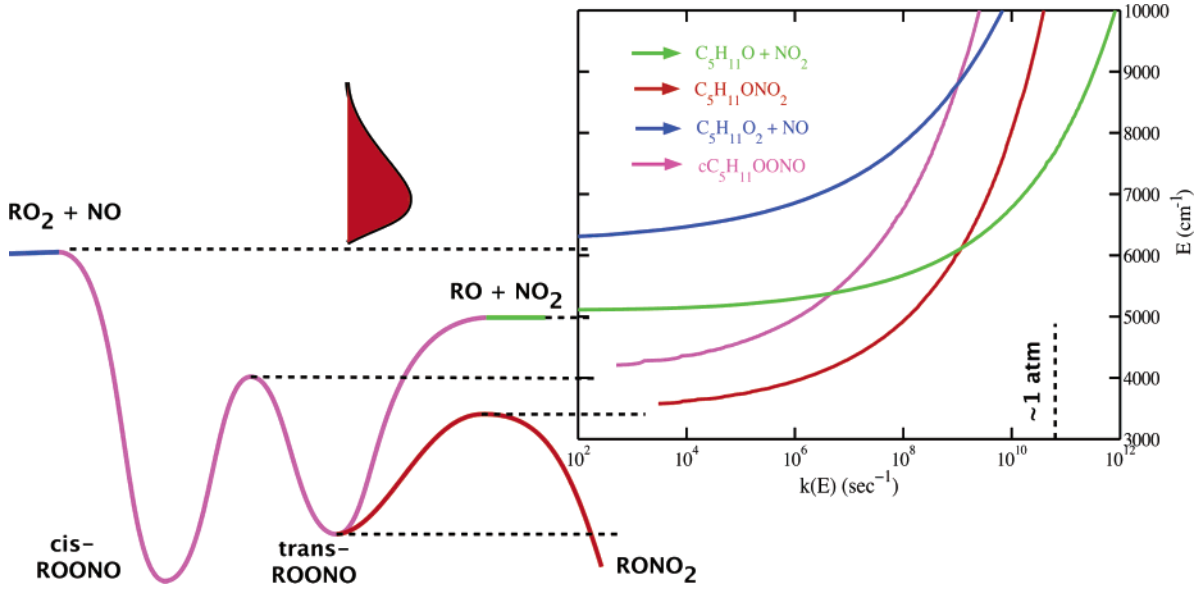


**Figure 6.** Microcanonical rate constants out of the *trans*-$C_5H_{11}OONO$ well, shown with the zero point corrected potential energy surface for context. The back reaction to reactants and the isomerization to *cis*-$C_5H_{11}OONO$ contribute negligibly at all energies. Production of radicals (RO + $NO_2$) dominates at the initial reactant energy (indicated with a red Boltzmann distribution), while isomerization to the nitrate ($RONO_2$) dominates at low energies (typical of ROONO thermal decomposition).

state regimes:[33] the "pseudo" steady state neglecting thermal decomposition and the "true" steady state including thermal decomposition of the intermediate. In our case, both ROONO intermediates are extremely short-lived for $T > 200$ K, so consideration of thermal decomposition is appropriate.

We determine the energy transfer matrix **P** from an upper level, *u*, to a lower level, *l*, using an "exponential down" model, with upward transitions (from *l* to *u*) determined through detailed balance:

$$P_{lu} = N_u\left(\frac{\rho_l\,\delta e_l}{\rho_u\,\delta e_u}\right)\exp\left(\frac{-\Delta E_{ul}}{E_D}\right) \quad (l \le u) \tag{12}$$

$$P_{ul} = P_{lu}\left(\frac{\rho_u\,\delta e_u}{\rho_l\,\delta e_l}\right)\exp\left(\frac{-\Delta E_{ul}}{kT}\right) \quad (l > u) \tag{13}$$

Normalization applies to *columns* of the transfer matrix, ensuring a unit probability that collisions will preserve the total population. Note that we include a variable energy grain size, $\delta e$; this allows us to maintain high energy resolution near critical energies and, if desired, near zero-point energies, thus improving the overall accuracy of the calculation without generating overly large matrices.[32] We typically employ a high-resolution grain of 10 $cm^{-1}$ and a lower resolution grain of 120.5 $cm^{-1}$.

Given the population **N**, we then find the yield *Y* for the *i*th channel:

$$Y_i(t) = \frac{\sum_E \mathbf{N}(E, t)\mathbf{K}_i(E)}{R} \tag{14}$$

## 5. Results

**5.1. The ROONO Well.** For our first set of results, we shall focus on the yield of nitrate ($RONO_2$) versus radicals (RO + $NO_2$) out of our model $C_5$ *trans*-ROONO system. We assume that all $RONO_2$ formed from ROONO isomerization is stabilized (this will be discussed below). These yields are shown as a function of collision frequency at 300 K in Figure 7. We use $E_D = 600$ $cm^{-1}$ for all the calculations below. The salient features are that only nitrate formation and radical production

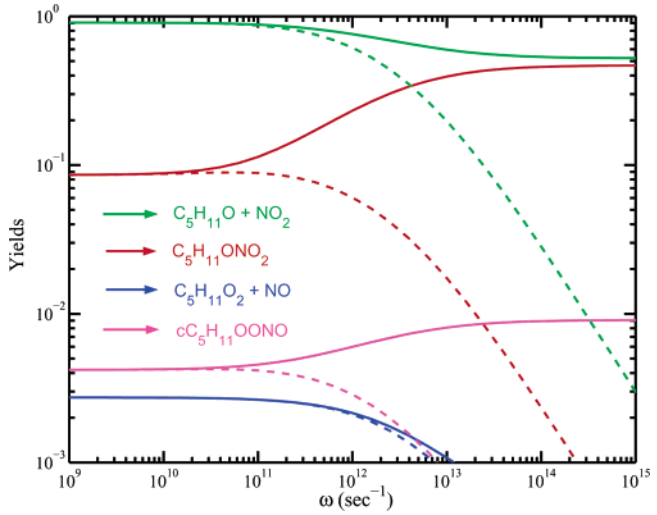


**Figure 7.** Product yields vs collision frequency out of $C_5$ *trans*-ROONO at 300 K for $E_D = 600$ $cm^{-1}$. Radicals (RO + $NO_2$) dominate at low pressure, but nitrate ($RONO_2$) maintains a 10% low-pressure asymptote. At high pressure, thermal decomposition of the ROONO dominates, and the two major yields are nearly identical. Two other pathways are insignificant (always below 1%). There is a very limited isomerization flux to *cis*-ROONO and an even lower back-flux to reactants. The collision frequency at 1 atm pressure is $\simeq 7 \times 10^{10}$ Hz. The dashed lines show yields neglecting thermal decomposition of the ROONO intermediate. ROONO stabilization, which is not shown, dominates above $\simeq 10^{13}$ Hz.

are important; neither reactant reformation nor isomerization to *cis*-ROONO is at all significant. There is a clear dependence on pressure (collision frequency), with radical production dominating at low pressure and the two channels competing equally at high pressure. About 10% of the flux yields nitrates even at very low pressure. Pseudo-steady-state results are shown in Figure 7 with dashed lines; these are clearly inconsistent with observations.

We next show the temperature dependence of these yields in Figure 8. The results are in clear qualitative agreement with the data shown in Figure 2, provided that we include thermal decomposition of the ROONO. There is a strong temperature

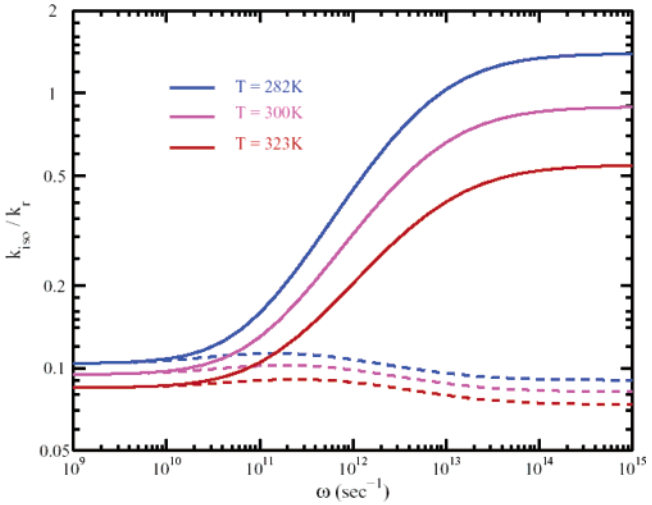


**Figure 8.** Branching ratio ($k_{iso}/k_r$) vs collision frequency out of $C_5$ *trans*-ROONO at three temperatures ($T$ = 282, 300, and 323 K). Results are shown with (solid lines) and without (dashed lines) considering thermal decomposition of stabilized *trans*-ROONO intermediates. The qualitative features seen in Figure 2 are reproduced here only with consideration of ROONO collisional stabilization. These include a low-pressure asymptote for nitrate formation and a strong temperature dependence at the high-pressure limit. The collision frequency at 1 atm pressure is $\simeq 7 \times 10^{10}$ Hz; this is the approximate center of the falloff curves shown in Figure 2. The center of the falloff curves shown here is $\simeq 3 \times 10^{12}$ Hz, which is not in good agreement.

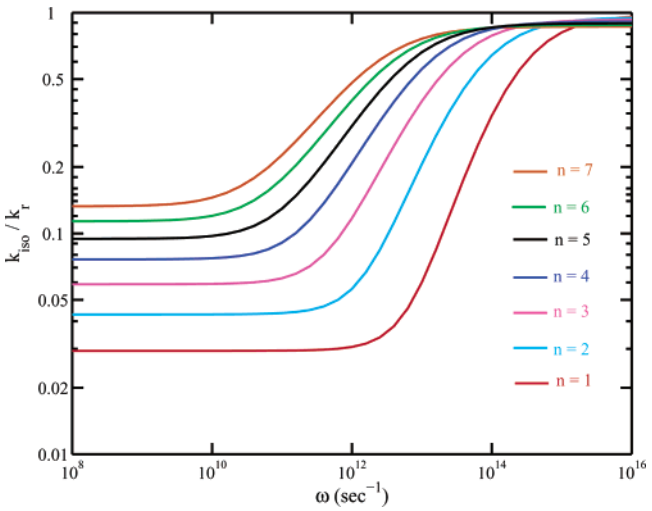


**Figure 9.** Branching ratio ($k_{iso}/k_r$) vs pressure for $C_1-C_7$ model systems. Results are shown with correction for adiabatic rotational modes. High-pressure limits are nearly identical. The falloff shifts to lower collisional frequency with increasing carbon number, as expected. Also, as carbon number and the number of energy storing modes increase, the low-pressure limit to nitrate production increases as well (at the logical limit of $C_\infty$ stabilization does not depend on external pressure).

dependence to the high-pressure asymptote, as well as a low-pressure asymptote consistent with the low-pressure behavior already discussed.

A second general feature of the data presented in Figure 5 was the tendency of the falloff behavior to shift by a factor of approximately 2.5 in pressure for each added carbon (based on a $C_5$ reference). The falloff behavior for systems ranging from $C_1$ to $C_7$ is shown in Figure 9. In all cases, we used the identical potential energy surface, simply changing the number of $CH_2$ groups in the model compound, as discussed earlier. The broad conclusion from this figure is that the collision frequency

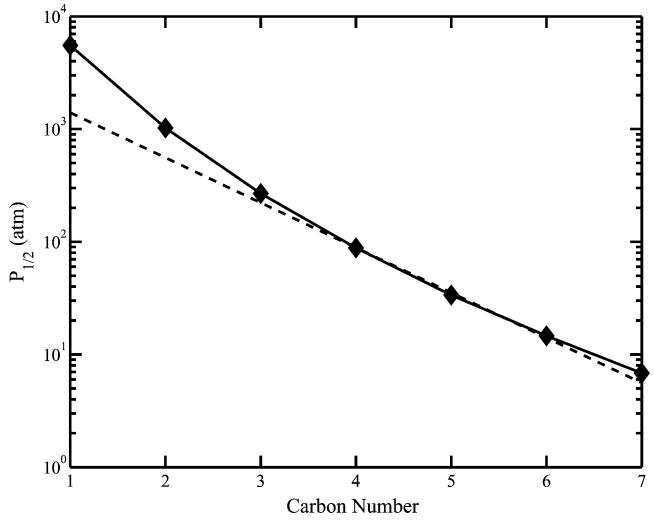


**Figure 10.** Pressure at the center of the falloff curve for nitrate yields vs carbon number. The dashed line has the slope of −2.5.

required to stabilize the ROONO drops with increasing carbon number (this is expected) and that the low-pressure limit for nitrate yields increases with carbon number as well. This second result is also expected, though somewhat less well-known. In essence, increasing the number of internal modes provides the reactive system with a well-coupled heat bath, which will eventually replace the need for collisional stabilization at high enough carbon number.

For each of the master equation results from $C_1$ to $C_7$, we can find the center of the falloff curve. The immediate result is a collision frequency where stabilization is 50% efficient, which we convert to a pressure with Lennard-Jones collision frequency relation:[35,36]

$$\omega = \Omega_{A-M}^{(2-2)*} \pi [(\sigma_A + \sigma_M)/2]^2 P \, \mathrm{Na} \sqrt{\frac{8}{\pi \mu k_B T}} \qquad (15)$$

with

$$\Omega_{A-M}^{(2-2)*} = [0.636 + 0.567 \log_{10}(k_B T/\epsilon_{A-M})]^{-1} \qquad (16)$$

which is accurate within ±7% in the range $0.3 \le k_B T/\epsilon_{A-M} \le 500$, or

$$\Omega_{A-M}^{(2-2)*} = [0.697 + 0.5185 \log(k_B T/\epsilon_{A-M})]^{-1} \qquad (17)$$

which is accurate within ±2.5% in the range $3 \le k_B T/\epsilon_{A-M} \le 300$. In the equations, $\sigma_A$ and $\sigma_M$ are size of *trans*-ROONO and the bath gas, respectively, Na is Avogadro's constant, $\mu$ is the reduced mass of the bath gas and trans-ROONO, and $\epsilon_{A-M} = (\epsilon_{A-A}\epsilon_{M-M})^{1/2}$, which is the Lennard-Jones well depth. The results are shown in Figure 10 as $P_{1/2}$ versus carbon number. The dashed black line in the figure has a slope of −2.5, equivalent to the result shown in Figure 5.

Figure 9 also shows that the low-pressure asymptote of the branching ratio ($k_{iso}/k_r$) increases with increasing carbon number. We plot in Figure 11 the low-pressure asymptote of $k_{iso}/k_r$ as a function of carbon number, which shows that the low-pressure asymptote of the branching ratio increases linearly with increasing carbon number.

**5.2. The $RONO_2$ Well.** Next, we must address the question of nitrate collisional stabilization. Up to now, we have been assuming that all nitrate is stabilized, but of course at low pressure vibrationally excited nitrate will itself decompose into

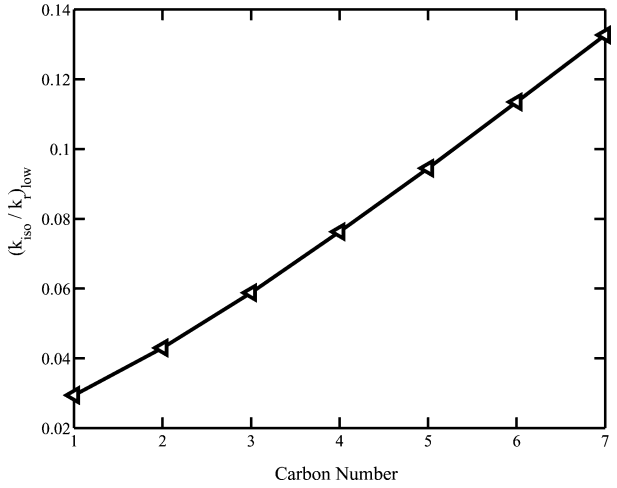


**Figure 11.** Low-pressure asymptote of the branching ratio ($k_{iso}/k_r$) vs carbon number. The low-pressure asymptote of $k_{iso}/k_r$ shows a linear dependence on the carbon number with $(k_{iso}/k_r)_{low} = 0.0174 \times C\# + 0.0088$ and $R^2 = 0.997$.

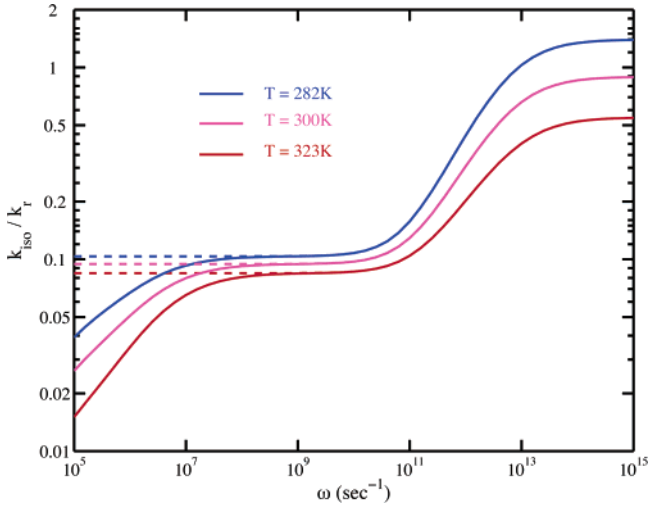


**Figure 12.** Branching ratio ($k_{iso}/k_r$) from $C_5$ *trans*-ROONO, including the effect of collisional stabilization of excited $RONO_2$. Without considering $RONO_2$ stabilization, $k_{iso}/k_r$ values remain constant at low pressure (dashed lines), while with this consideration they drop off after a plateau lasting approximately a factor of 1000 in pressure.

the same radical products as ROONO (RO + $NO_2$). Fortunately, the back flux from excited $RONO_2$ to ROONO is trivially small, so we can continue to treat the problem as a cascade of wells, using the energy-dependent flux out of one well to initialize the next. Because the nitrate well is *much* deeper than the ROONO wells, the vibrationally excited intermediates will be much longer lived, and stabilization will occur at a much lower pressure than in the ROONO case just shown. Our model for nitrate decomposition was discussed above as we described our microcanonical rate constants. The effect of considering this additional stabilization event is shown in Figure 12 for our $C_5$ model system. As expected, branching ratios show an additional falloff with reduced collisional frequency, this time at very low frequency (less than a few Torr pressure). We thus expect these multiwell systems to display a characteristic double falloff behavior if studied over a sufficiently wide pressure range. The result also suggests dramatically reduced nitrate yields for small systems that lie in the second falloff at a given pressure (for example, $C_1$ and $C_2$ systems).

**5.3. Cis−Trans ROONO Branching.** Finally, we must consider the cis−trans branching ratio of the initial $RO_2$ + NO reaction. In our model, only *trans*-ROONO leads to $RONO_2$, and we have shown that there is essentially no cis−trans interconversion. So, by adding *cis*-ROONO, we decrease the $RONO_2$ yield proportionally. This is shown in Figure 13. Once we include this initial branching, the logical abscissa is once again nitrate yield, as opposed to the $k_{iso}/k_r$ abscissa we have been employing. We have no reason to believe that the cis−trans branching ratio differs markedly from 50/50, so we have held it to this figure (unit production of *trans*-ROONO is shown with the dashed lines, 50/50 cis/trans production is shown with the solid lines). Of course, this branching ratio affects the overall yield of nitrates quite markedly; one intriguing possibility is that this is the reason for the systematic difference in nitrate production among different classes of peroxy radicals.

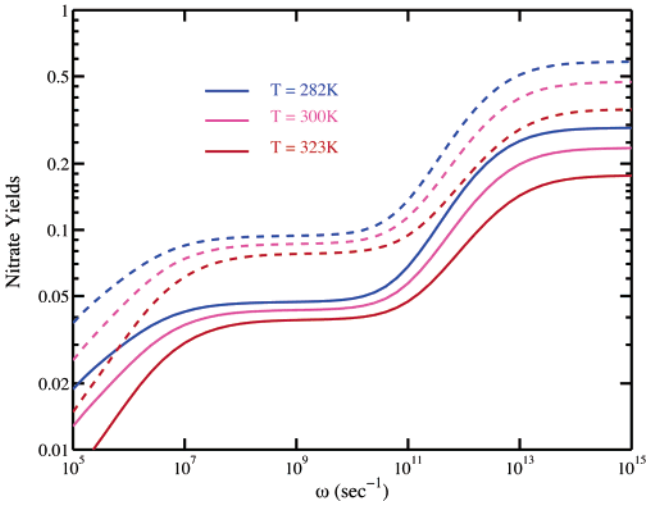


**Figure 13.** Yields of nitrate from $C_5$ $RO_2$ + NO, including cis−trans branching of the ROONO formation. The dashed lines are the earlier result for pure *trans*-ROONO, while the solid lines show the effect of a 50−50 cis−trans branching, with *cis*-ROONO leading exclusively to RO + $NO_2$.

## 6. Discussion

**6.1. Comparison with Literature Data.** Our model successfully reproduces the observed nitrate production, including the temperature, pressure, and size (carbon number) dependence and including both high- and low-pressure asymptotes. Specifically,

1. The pressure dependence of nitrate yields ($k_{iso}/k_r$) takes the form of a sigmoid, with a low-pressure limit of order 0.05 and a high-pressure limit of order 1.

2. The temperature dependence of the high-pressure limits is steep and negative, with nitrate yields increasing sharply with decreasing temperature. The basic temperature dependence is determined by the energy difference between the two transition states, which we constrain based on observed temperature dependences, so this result is expected.

3. The center of each falloff curve shifts with carbon number, consistent with the observed $2.5^{C\#}$ dependence. This result is not influenced by any parameter adjustment. Other results go beyond any observational constraint. These include the following:

1. The low-pressure asymptote shows a strong carbon number dependence, with a yield of 0.03 (*trans*-ROONO pathway only) for $C_1$ (a model-world $C_1$ secondary peroxy radical), increasing steadily to a yield of 0.13 for $C_7$.

2. A significant pressure dependence is only achieved if collisional stabilization of the ROONO intermediate is included.

3. A second pressure falloff lies at very low pressure. This corresponds to collisional stabilization of the vibrationally excited $RONO_2$ product, but it will only have atmospheric significance for $C_1$ and perhaps $C_2$ systems.

4. The nitrate yields are very sensitive to the *cis*- and *trans*-ROONO yields. No current data can constrain this. However, the few available low-temperature data for cycloalkenes[37] clearly indicate that nitrate production does not become asymptotically dominant at low temperature, as a naïve extrapolation (i.e., Figure 3) might suggest. It is thus a general success of this model that it caps the possible nitrate yields. The beginning of this capping effect is visible at the high-pressure end of Figure 13, where the distance between the 282 and 300 K lines is significantly less than the distance between the 300 and 323 K lines when cis−trans branching is included.

There is one very important exception to the generally good agreement with experimental data; the absolute pressure required for a given degree of stabilization in our model is at least an order of magnitude higher than in the data. However, it is possible to reconcile the model with observations at the extreme limit of some highly uncertain parameters; we shall return to this subject after revisiting the data parametrization below. All of these parameters are extremely uncertain, and at the moment there is essentially no basis for experimental comparison. Most notably, we cannot draw on kinetics of the RO + $NO_2$ reaction, as these data ultimately constrain only the total nitrate formation and thus do not constrain the ROONO radical channel to any significant extent. The exception is the OH + $NO_2$ system, which is now sufficiently rich with data over a wide pressure and temperature range to elucidate the full mechanism but which is unfortunately removed from the systems under consideration here by both the degree of substitution and the actual energetics of the potential energy surface.

**6.2. Validity of the Model System.** We must emphasize that we are treating this problem with a relatively crude model system. Notably crude assumptions include the following:

1. We make no effort to consider changes to the potential energy surface with increased carbon number; we simply add modes consistent with the behavior of a $CH_2$ group with each added carbon. We *do* specifically model changes to the moment of inertia difference between ROONO and the transition states, which become insignificant with increasing carbon number.

2. We assume that the ROONO species can be neatly classified according to their O−O−N−O conformation (cis or trans) and that only these two conformers are significantly different. Again, we assume that this distinction holds for all carbon numbers.

3. We assume that only *trans*-ROONO couples to nitrate production.

We feel that each of these assumptions is well justified, but we have also chosen them to illustrate a limiting case. For example, it is certain that formal transition states exist from any ROONO conformer to $RONO_2$, but the theoretical accuracy of any computational transition state appears to remain poor. Our primary assertion is that these transition state energies are very likely different, and so we are exploring the limiting case in which only one transition state plays a significant role. Considering any more than two conformers of ROONO would only cloud the picture. Likewise, the available data on the thermochemistry of organic nitrates are generally consistent with our first assumption. Broadly, we do not expect these computational results to be quantitatively accurate, but we do assert that they provide a framework for consideration of data spanning a much wider range in pressure, temperature, and carbon number than the currently available data set.

**6.3. Comparison with Model Studies.** Our conclusions about this system differ from the recent study by Barker et al.[14] in two primary ways: (1) we explicitly consider two separate ROONO conformers, and (2) we assume that the major cause of the observed pressure dependence is collisional stabilization in the ROONO well, while they conclude that stabilization in the $RONO_2$ well is responsible for the observed pressure dependence. The potential energy surfaces and transition state structures used in both studies are substantially similar; most notably, the critical energy difference between the isomerization and radical pathways is nearly the same. *Both* studies are substantially challenged with quantitative treatment of the pressure dependence. Simply put, for the pressure dependence to be due to $ROONO_2$ stabilization, a surprisingly small $E_D$ of 25 $cm^{-1}$ is required,[14] while for ROONO stabilization to be the cause we need to combine an unusually slow dissociation reaction with an unusually *large* $E_D$. In our opinion, neither result is fully satisfying, and they are equally likely to prove correct. As Barker et al. clearly discuss, there is ample room for parameters in these models to adjust for other errors, most notably inaccuracies in the very poorly constrained transition states. Thus, one "unphysical" parameter may simply reflect errors in another. Of course, an unexplored mechanism may ultimately prove to be in effect; ultimately, only a greatly expanded data set will sufficiently constrain these models for them to provide predictive accuracy.

There is one compelling result that favors our model. The carbon number dependence of the low-pressure asymptotes is an almost inevitable consequence of chemical physics, provided that internal energy transfer is rapid and the systems are behaving statistically (and there is *no* reason to doubt this). As the number of active internal modes grows, chemically activated systems will behave more and more thermally, simply because the internal heat bath (comprising the modes orthogonal to the reaction coordinate) has a progressively higher heat capacity. If the basic pressure dependence observed in nitrate production were due to stabilization of the secondary product (the chemically activated $RONO_2$), the high-pressure limits of those yields would be equivalent to the intermediate plateau of our results (i.e., Figure 12), *and this value depends strongly on carbon number* (Figure 9). The variation is almost a factor of 2 from $C_4$ to $C_7$, and there is no evidence of such variability in the empirical pressure falloff fits (Figure 2).

The critical issues raised in this study are the possibly different roles of the ROONO conformers and the assertion that *eventually*, collisional stabilization of the ROONO will come into play. As we discussed above, one clear implication of distinct ROONO conformers is that nitrate production will be capped at low temperature, with unit production only from those channels that actually couple to nitrate; this is clearly consistent with the limited available low-temperature data and resolves a serious flaw in the existing *interpolation* schemes when they are used to *extrapolate* yields to low temperatures.

Our conclusion differs from that of Zhao et al.[16] in one significant aspect. We have shown that the *cis*- and *trans*-ROONO conformers are effectively distinct, assuming a 4200 $cm^{-1}$ cis−trans isomerization barrier. They calculate a lower barrier (3500 $cm^{-1}$) and assert that interconversion will be rapid. This is *not* necessarily true; for example, one can see in Figure 6 that even at this low energy for TS1, this isomerization will be slower than either $RONO_2$ or RO + $NO_2$ formation at all energies. However, it *is* true that the conformer not directly

coupled to $RONO_2$ would favor isomerization to dissociation at low temperature. To the extent that data indicate that dissociation remains important at low temperature, the higher barrier is consistent with the data.

Concerning ROONO stabilization, if we take the results from Figure 9 at face value, we should see stabilization of ROONO at a carbon number near $C_{15}$, at which point the *low*-pressure asymptote will also include a very substantial (~50%) nitrate yield. This has clear implications for the oxidation mechanisms of large hydrocarbons associated with secondary organic aerosol (SOA) production, where low-volatility nitrates could be an important component of SOA in high-NOx environments.

**6.4. Parametrizations.** The existing parametrization for nitrate production[1,3] successfully fits most available data over the pressure and temperature range covered (100−700 Torr, 282−323 K), but in our opinion it has three significant flaws: (1) by not including "closed" channels (with respect to nitrate production), it overpredicts nitrate yields at low temperature; (2) the $(T/300)^{-n}$ form for the high-pressure temperature dependence is inconsistent with thermal decomposition of the ROONO intermediate, which demands an Arrhenius form; and (3) it fails to reproduce the low-pressure asymptote evident in the data. To rectify these deficiencies, we propose an alternate parametrization as follows. The overall nitrate yield can be seen as a product of the branching ratio, $\alpha$, between "open" and "closed" (to nitrate production) pathways and the specific yield, $\beta$, of nitrate in the open pathway:

$$Y = \alpha\beta \tag{18}$$

Our best guess, with few current constraints, is that $\alpha \simeq 0.5$. The specific yield is best understood in terms of competitive rate constants $k_r$ and $k_{iso}$:

$$\beta = \frac{k_{iso}}{k_r + k_{iso}} = \frac{1}{1 + (k_{iso}/k_r)^{-1}} \tag{19}$$

Finally, the term $k_{iso}/k_r$ is what we have modeled in our simulations. This can be parametrized as a standard pressure falloff with a nonzero (bimolecular) low-pressure limit:

$$\frac{k_{iso}}{k_r} = r = r_{low} + \frac{r_\infty - r_{low}}{1 + [M_c]/[M]} F([M_c]/[M]) \tag{20}$$

The broadening function (for $F_c$ near unity) is adequately expressed as a simplified form of Troe's falloff parametrization.[24,38,39]

$$F([M_c]/[M]) = F_c^{\{1+[\log_{10}([M_c]/[M])]^2\}^{-1}} \tag{21}$$

This is identical to the form used by the IUPAC kinetics parametrization.[40] Because the pressure falloff behavior reflects *thermal* decomposition, an Arrhenius form best describes the temperature dependence:

$$r_\infty = A_\infty \, e^{-(\theta_\infty/T)} \tag{22}$$

The center of the falloff curve does *not* depend on temperature in the simplest model (nor does it in our master equation results), but a dependence can be included if necessary. However, $[M_c]$ clearly depends on the carbon number.

$$[M_c] = [Mc300](T/300)^{-m} S^{(5-C\#)} \tag{23}$$

We use a $T^{-m}$ dependence because the primary source of a temperature dependence to $[M_c]$ will be changes to the collisional frequency and efficiency. The simple $S^{(5-C\#)}$ form will probably *not* be adequate for very large carbon numbers, when data become available. Finally, the low-pressure limit will have a temperature and carbon number dependence

$$r_{low} = r_{l300}(T/300)^{-n}(1 + L(C\# - 5)) \tag{24}$$

Again, the carbon number dependence will probably not extrapolate well to very large carbon number, but there are no data to provide a good constraint. Logically, $r_{low}$ would approach $r_\infty$ as the carbon number approached $\infty$.

All told, this parametrization has the following free parameters: $\alpha$, $F_c$, $A_\infty$, $\theta_\infty$, Mc300, $m$, $S$, $r_{l300}$, $n$, and $L$. Not all of these parameters are well constrained by current data. Specifically, $\{\alpha, F_c, m\}$ are at best loosely constrained. For now, we shall assume $\alpha = 0.5$. Our estimate of $F_c$ is based on an analysis of the master equation falloff curves as follows.[24,38,39,41] We find the intercept of the linearly increasing low-pressure yields with the high-pressure asymptote. This identifies $\omega_c$. A Lindemann−Hinschelwood system would show $r = 0.5r_\infty$ at this point. The value of $F_c$ is thus $2r_{\omega_c}/r_\infty$. The average from $C_1$ to $C_7$ is $F_c = 0.7$.

There are several salient aspects to the fitting. One is that it is very difficult, with many local minima and only a shallow global minimum. This is because many of the parameters are highly correlated, but also because the data also have a lot of hidden covariance, especially among groups such as the heptyl$ONO_2$; the specific yields depend on branching ratio estimates for the primary oxidation reaction. A second aspect is that the many local minima imply that multiple solutions are difficult to differentiate purely on the basis of a least-squares minimum.

Our approach is to constrain most of the parameters based on theory and only optimize a few parameters at a time. For this, we used a constrained least squares optimization method described earlier.[42] We use theoretical constraints for most parameters where there is little constraint from the data and a certain amount of judgment in some intermediate cases; for example, the data are consistent with the parameter $L$ (low-pressure carbon number dependence) equal to 0.2 instead of the theoretically constrained 0.17 shown in Figure 11. The final result is not a global minimum but rather a "good" result, one that reproduces all of the qualitative behavior of the system with less bias and error than the currently accepted parametrization.[3]

Our final parameter set is $\alpha = 0.5$, $F_c = 0.7$, $A_\infty = 0.025$, $\theta_\infty = -1565$ K, Mc300 $= 3.821 \times 10^{20}$, $m = 0$, $S = 2.5$, $r_{l300} = 0.075$, $n = 1$, and $L = 0.2$. We do not report uncertainties with these parameters, as that would be meaningless. The resulting yield function, together with the $C_5$, $C_6$, and $C_7$ data, is shown in Figure 14. From the two figures, we can see that this function describes the general behavior of the data quite well, though individual data fall relatively far from the average curve. While this function is only marginally better than the currently accepted parametrization as an *interpolation* function, it differs dramatically in extrapolation, especially at low pressure and at high pressure and low temperature. The high-pressure, low-temperature difference has the most practical significance, as it will substantially alter model behavior in low-temperature regions of the atmosphere.

**6.5. Revised Microcanonical System.** The fitting result also reveals a much higher $A$-factor ratio and much lower $\theta$ than the original simple analysis presented in the beginning of the paper. $A$ is now 0.025, and $\theta$ is −1565 K. This suggests that the isomerization transition state is only marginally tighter than

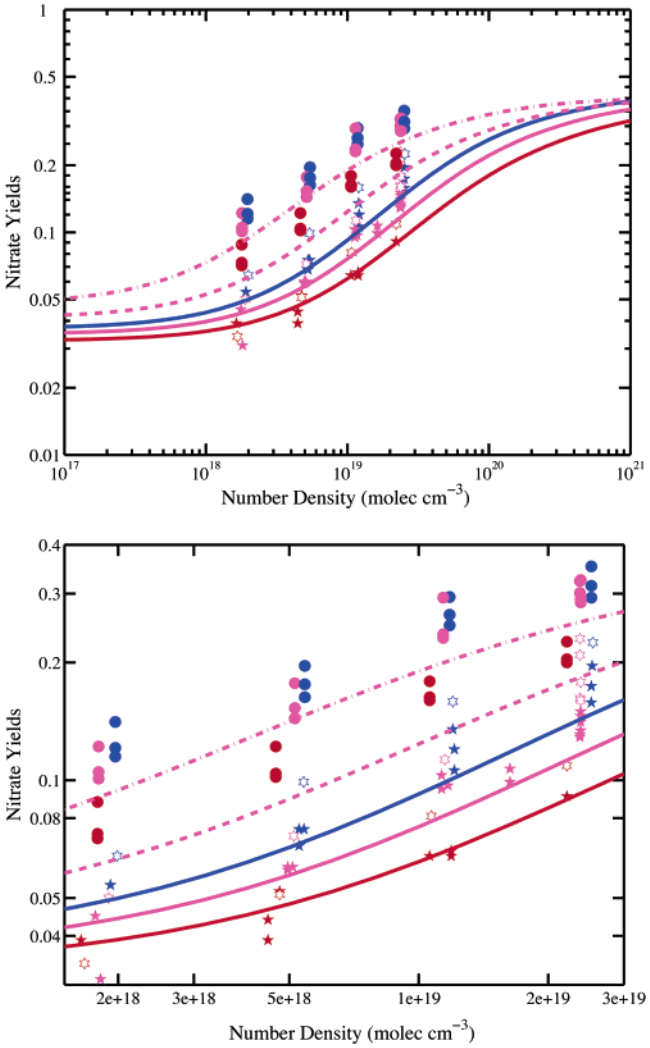


**Figure 14.** Nitrate yields vs number density (pressure) for the model and all the $C_5$, $C_6$, and $C_7$ data of secondary peroxy radicals reacting with NO by Atkinson (ref 3), over a broad and narrow pressure range. The symbol shape shows the carbon number in the peroxy radical: solid five-pointed stars for $C_5$ peroxy radicals, including 2-pentyl, 3-pentyl, and 2-methyl-3-butyl peroxy radicals; six-pointed stars for $C_6$ peroxy radicals, including 2-hexyl, 3-hexyl, and 3-methyl-2-pentyl peroxy radicals; and solid circles for $C_7$ peroxy radicals, including 2-heptyl, 3-heptyl, and 4-heptyl peroxy radicals. The edge color of each symbol corresponds to temperature: blue for 282 K; magenta for 300 K; red for 323 K. The lines in the figure are our interpolation function: the solids lines are for $C_5$ peroxy radicals at 282 K (in blue), 300 K (in magenta), and 323 K (in red); the dashed magenta line is for $C_6$ peroxy radicals at 300 K; and the dashed−dotted magenta line is for $C_7$ peroxy radicals at 300 K.

the radical transition state, and the isomerization transition state is relatively close to the radical transition state energy. This is consistent with plausible chemical physics, with a transition state resembling dissociated radicals. Also, it hints at a resolution to the problem of the absolute pressure. While the obvious way to increase the *A*-factor is to loosen the isomerization transition state, it is also possible to *tighten* the radical transition state. This would drop the $k(E)$ for the radical pathway and might well get us into the ballpark of agreement with the data. In practice, we can obtain reasonable agreement with observations by tightening *both* transition states, increasing $\zeta$ (the "loosening factor" for the isomerization transition state) from 0.4 to 0.77 and decreasing $\gamma$ (the hindrance factor for ROONO decomposition) from 0.08 to 0.035 (corresponding to $(1 - \eta)^{1/2} \approx 0.07$ in the restricted Gorin model by Smith and Golden[30]). The

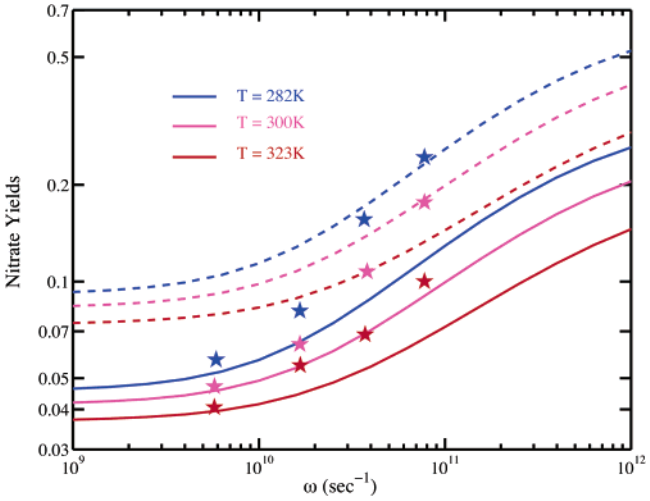


**Figure 15.** Master equation model results forced to good agreement with data for 2-methyl-3-butyl peroxy + NO. Both radical dissociation and nitrate isomerization transition states are significantly tightened, thus increasing the microcanonical lifetime of the excited intermediate and facilitating collisional stabilization.

*A*-factors for reactions 2 and 3 now are $2.2 \times 10^{15}$ and $6.6 \times 10^{12}$ s$^{-1}$, respectively, giving an *A*-factor ratio of 0.003. While this is lower than our parametrization fit (0.025), we also use a lower critical energy in the master equation model (−2200 K as opposed to −1565 K in the parametrization). These values are covariant, and both pairs are reasonably consistent with the relation expressed in Figure 4. The resulting $C_5$ model agrees quite well with data for the 2-methyl-3-butyl peroxy + NO reaction, as shown in Figure 15.

In the resulting model, the ratio of *A*-factors for the reverse reactions of RO + $NO_2$ forming various ROONO and $RONO_2$ is 0.3:1. Others have assumed that this ratio should be of order 2:1,[14] a reasonable assumption consistent with what we know about the analogous OH + $NO_2$ reaction. However, there is no direct experimental evidence supporting this claim, and it is certainly possible that specific effects, such as nonadiabatic interactions of mixed excited states (i.e., a conical intersection), *could* slow decomposition of the *trans*-ROONO intermediate.[17] Indeed, even the evidence from the OH + $NO_2$ system does not preclude this possibility. Double exponential decays observed in high-pressure OH + $NO_2$ recombination[43] only show that *some* HOONO intermediate is formed with a rate constant similar to that of $HONO_2$ formation. The calculated equilibrium constants for the presumed HOONO intermediate are quite consistent with theoretical *cis*-HOONO bond energies,[43] so it is entirely possible that even the OH + $NO_2$ system does not produce the *trans*-HOONO intermediate efficiently. In summary, to force our model to come into reasonable accord with nitrate yield data, we have chosen to postulate a transition state with few, if any, experimental or theoretical constraints.

At this point, we should clearly articulate the different approaches and objectives of our study from Barker and Lohr.[14] Both studies consider the same general system, but from differing perspectives. In particular, Barker and Lohr use a "best available" computational surface and constraints from a secondary reaction (the RO + $NO_2$ recombination) to develop a model for nitrate formation from $RO_2$ + NO. Given the correlated uncertainties in energy transfer parameters and transition state properties, they argue that this may reflect errors in the transition states. Our objective is to use easily accessible theory (density functional computations and the master equation) to serve as a guide for interpretation of existing nitrate yield data, focusing

in particular on the pressure, temperature, and carbon number dependence and accepting all aspects of the only data set with significant coverage in this parameter space.[23] Important features turn out to be the low-pressure asymptote in yields (expressed as a positive artifact in the lowest pressure yield data when all data are subject to a standard pressure falloff fit) and the constant (with carbon number) high-pressure yield asymptote. We regard the transition state properties leading to radical products and nitrates out of the *trans*-ROONO well as substantially unconstrained and consequently adjust those parameters to arrive at a result that is consistent with the available data. Both studies have a common conclusion: the existing data set is insufficient to constrain this system. At a minimum, data for higher carbon numbers, higher pressures, and lower temperatures are required to isolate key effects. Far better would be experiments specifically designed to isolate the ROONO intermediate itself.

## 7. Conclusions

We have presented a model for nitrate ($RONO_2$) yields from $RO_2 + NO$ reactions that describes all of the salient features of the observed pressure, temperature, and carbon number dependence in experimental systems. This model relies on four critical assumptions:

1. The pressure dependence of nitrate yields reflects collisional stabilization of short-lived peroxynitrite (ROONO) intermediates.

2. The peroxynitrite intermediates are produced in at least two distinct conformations, which do not readily interconvert. Only one of these forms (here called *trans*-ROONO) leads to significant $RONO_2$ production.

3. The temperature dependence of nitrate yields reflects the thermal decomposition of the peroxynitrite intermediates.

4. The basic potential energy surface for systems larger than $C_2$ remains largely unchanged as carbon number increases.

Given these assumptions, we draw the following conclusions, several of which differ from previously published assessments of this system:

1. Nitrate yields display a dual falloff curve, with a high-pressure asymptote caused by full stabilization of the ROONO intermediate, an intermediate pressure plateau caused by negligible stabilization of the ROONO but full stabilization of the resulting $RONO_2$ product, and a low-pressure falloff as $RONO_2$ stabilization itself becomes inefficient.

2. The observed pressure dependence in systems larger than $C_4$ is due to the second rise of this dual falloff, between the plateau region and the high-pressure asymptote. This explains the ubiquitous deviation of lower pressure yield data from a simple falloff curve.

3. The intermediate pressure plateau shows a strong carbon number dependence in nitrate production, while the high-pressure asymptote is independent of carbon number.

4. The very small yields observed in small systems ($C_1$ and $C_2$) lie in the low-pressure falloff regime of the double falloff curve.

5. The high-pressure limits of nitrate production rise with decreasing temperature, but they are capped by the branching ratio for *cis*- and *trans*-ROONO formation, which is not well constrained by experiment. Assuming a roughly 50−50 cis−trans branching ratio, the maximum possible nitrate yield is 50%.

Based on these results, we have presented a new parametrization for nitrate production, considering only ROONO stabilization (it is thus not appropriate for very low carbon numbers). This parametrization includes the cis/trans branching, a low-pressure asymptote that depends on carbon number, and an Arrhenius form for the high-pressure limit driven by thermal decomposition of the intermediate. The parametrization is roughly equivalent to existing parametrizations for interpolation but differs dramatically in extrapolation, where there are no constraints from data but where our theoretical considerations provide guidance. Most notably, the cap in low-temperature yields will affect global model calculations. As new laboratory data emerge, we will be able to test the limits of this model, in particular constraining the high carbon number, low-temperature regime and the hypothesis, presented here, that changes in nitrate production for R-groups with different degrees of substitution (i.e., primary, secondary, tertiary, and hydroxy-substituted peroxy radicals) are due largely to changes in the initial cis/trans branching ratio for peroxynitrite production.

**Acknowledgment.** This work is supported by Grant ATM-0125283 from the National Science Foundation. We thank Michele Sprengnether and John Barker for valuable discussion and comments. We also thank Judea Goins for early work on the nitrate yield data.

**Supporting Information Available:** Geometries and frequencies for all stable species and the transition state between *trans*- and *cis*-ROONO intermediates of the $RO_2 + NO$ reaction system for R = H, $CH_3$, $C_2H_5$, *n*-$C_3H_7$, *i*-$C_3H_7$, and 2-$C_5H_{11}$ optimized at the B3LYP/6-31+G(d,p) level of theory by Gaussian98; moments of inertia for *trans*-ROONO and for the fragments of $RO_2$ and NO, RO and $NO_2$ in three dimensions for the dissociation reaction with R = $CH_3$, $C_2H_5$, *n*-$C_3H_7$, *i*-$C_3H_7$, and 2-$C_5H_{11}$; moments of inertia for $RONO_2$ and for the fragments of RO and $NO_2$ in three dimensions for the dissociation reaction with R = $CH_3$, $C_2H_5$, *n*-$C_3H_7$, *i*-$C_3H_7$, and 2-$C_5H_{11}$. This material is available free of charge via the Internet at http://pubs.acs.org.

## References and Notes

(1) Atkinson, R.; Aschmann, S. M.; Winer, A. M. *J. Atmos. Chem.* **1987**, *5*, 91.

(2) Atkinson, R. *J. Phys. Chem. Ref. Data* **1994**, *Monograph 2*, 216.

(3) Carter, W. P. L.; Atkinson, R. *J. Atmos. Chem.* **1989**, *8*, 165.

(4) Chen, X.; Hulbert, D.; Shepson, P. B. *J. Geophys. Res.* **1998**, *103*, 25563.

(5) Sprengnether, M.; Demerjian, K. L.; Donahue, N. M.; Anderson, J. G. *J. Geophys. Res.* **2002**, *107*, 8-1-8-13.

(6) Chuong, B.; Stevens, P. S. *J. Geophys. Res.* **2002**, *107*, 2-1-2-12.

(7) Zhang, D.; Lei, W.; Zhang, R. *Chem. Phys. Lett.* **2002**, *358*, 171.

(8) Burkholder, J. B.; Hammer, P. D.; Howard, C. J. *J. Phys. Chem.* **1987**, *91*, 2136.

(9) Mcgrath, M. P.; Francl, M. M.; Rowland, F. S.; Hehre, W. J. *J. Phys. Chem.* **1988**, *92*, 5352.

(10) Li, Y.; Francisco, J. S. *J. Phys. Chem.* **2000**, *113*, 7976.

(11) Dixon, D. A.; Feller, D.; Zhan, C.; Francisco, J. S. *J. Phys. Chem. A* **2002**, *106*, 3191.

(12) Zhang, D.; Zhang, R. *J. Am. Chem. Soc.* **2002**, *124*, 9600.

(13) Lohr, L. L.; Barker, J. R.; Shroll, R. M. *J. Phys. Chem. A* **2003**, *107*, 7429.

(14) Barker, J. R.; Lohr, L. L.; Shroll, R. M.; Reading, S. *J. Phys. Chem. A* **2003**, *107*, 7434.

(15) Golden, D. M.; Barker, J. R.; Lohr, L. L. *J. Phys. Chem. A* **2003**, *107*, 11057.

(16) Zhao, Y.; Houk, K. N.; Olson, L. P. *J. Phys. Chem. A* **2004**, *108*, 5864.

(17) Ellison, G. B.; Herbert, J. M.; McCoy, A. B.; Szalay, P. G.; Stanton, J. F. *J. Phys. Chem. A*, in press.

(18) Chase, M. W. *NIST JANAF Thermochemical Tables, 4th ed.* (*Journal of Physical and Chemical Reference Data, Monograph, No. 9*); Technical Report; National Institute of Standards and Technology: Gaithersburg, MD, 1998.

(19) Sander, S. P.; Friedl, R. R.; DeMore, W. B.; Golden, D. M.; Kurylo, M. J.; Hampson, R. F.; Huie, R. E.; Moortgat, G. K.; Ravishankara, A. R.; Kolb, C. E.; Molina, M. J. *Chemical Kinetics and Photochemical Data for*

*Use in Stratospheric Modeling, Evaluation Number 13*; Technical Report 00-3; Jet Propulsion Laboratory: Pasadena, CA, 2000.

(20) Atkinson, R.; Baulch, D. L.; Cox, R. A.; Crowley, J. N.; Hampson, R. F.; Kerr, J. A.; Rossi, M. J.; Troe, J. *Summary of Evaluated Kinetic and Photochemical Data for Atmospheric Chemistry*; Technical Report, IUPAC Subcommittee on Gas Kinetic Data Evaluation for Atmospheric Chemistry, 2002 (http://www.iupac-kinetic.ch.cam.ac.uk/).

(21) Donahue, N. M.; Mohrschladt, R.; Dransfield, T. J.; Anderson, J. G.; Dubey, M. K. *J. Phys. Chem. A* **2001**, *105*, 1515.

(22) Dransfield, T. J.; Donahue, N. M.; Anderson, J. G. *J. Phys. Chem. A* **2001**, *105*, 1507.

(23) Atkinson, R.; Carter, W. P. L.; Winer, A. M. *J. Phys. Chem.* **1983**, *87*, 2012.

(24) Troe, J. *J. Phys. Chem.* **1979**, *83*, 114.

(25) Sander, S. P.; Friedl, R. R.; Huie, R. E.; Kurylo, M. J.; Orkin, V. L.; Kolb, C. E.; Moortgat, G. K.; Golden, D. M.; Ravishankara, A. R.; Molina, M. J.; FinlaysonPitts, B. J. *Chemical Kinetics and Photochemical Data for Use in Atmospheric Studies, Evaluation Number 14*; Technical Report 02-25; Jet Propulsion Laboratory: Pasadena, CA, 2002.

(26) Atkinson, R.; Aschmann, S. M.; Carter, W. P. L.; Winer, A. M. *J. Phys. Chem.* **1982**, *86*, 4563.

(27) Arey, J.; Aschmann, S. M.; Kwok, E. S. C.; Atkinson, R. *J. Atmos. Chem. A* **2001**, *105*, 1020.

(28) Abbatt, J. Studies of Gas-Phase Free-Radical Reactivity. Ph.D. Thesis, Harvard University, Cambridge, MA, 1990.

(29) Herschbach, D. R.; Johnston, H. S.; Pitzer, K. S.; Powell, R. E. *J. Chem. Phys.* **1956**, *25*, 736.

(30) Smith, G. P.; Golden, D. M. *Int. J. Chem. Kinet.* **1978**, *10*, 489.

(31) Benson, S. W. *Thermochemical Kinetics*; John Wiley & Sons: New York, 1976.

(32) Barker, J. R. *Int. J. Chem. Kinet.* **2001**, *33*, 232.

(33) Kroll, J. H.; Sahay, S. R.; Anderson, J. G.; Demerjian, K. L.; Donahue, N. M. *J. Phys. Chem. A* **2001**, *105*, 4446.

(34) Holbrook, K. A.; Pilling, M. J.; Robertson, S. H. *Unimolecular Reactions*; John Wiley & Sons: New York, 1996.

(35) Reid, R. C.; Sherwood, T. K. *The Properties of Gases and Liquids*, 2nd ed.; McGraw-Hill: New York, 1966.

(36) Troe, J. *J. Chem. Phys.* **1977**, *66*, 4758.

(37) Orlando, J. J.; Iraci, L. T.; Tyndall, G. S. *J. Phys. Chem. A* **2000**, *104*, 5072.

(38) Troe, J. *Ber. Bunsen-Ges. Phys. Chem.* **1974**, *78*, 478.

(39) Baulch, D. L.; Cox, R. A.; Hampson, R. F.; Kerr, J. A.; Troe, J.; Watson, R. T. *J. Phys. Chem. Ref. Data* **1980**, *9* (2), 295.

(40) Atkinson, R.; Baulch, D. L.; Cox, R. A.; Crowley, J. N.; Hampson, R. F.; Kerr, J. A.; Rossi, M. J.; Troe, J. *Summary of Evaluated Kinetic and Photochemical Data for Atmospheric Chemistry*; Technical Report, IUPAC Subcommittee on Gas Kinetic Data Evaluation for Atmospheric Chemistry, 2003 (http://www.iupac-kinetic.ch.cam.ac.uk/).

(41) Donahue, N. M.; Dubey, M. K.; Mohrschladt, R.; Demerjian, K.; Anderson, J. G. *J. Geophys. Res.* **1997**, *102*, 6159.

(42) Donahue, N. M.; Clarke, J. S. *Int. J. Chem. Kinet.* **2004**, *36* (5), 259.

(43) Hippler, H.; Nasterlack, S.; Striebel, F. *Phys. Chem. Chem. Phys.* **2002**, *4*, 2959.